scientific reports

Check for updates

OPEN

The plasma degradome reflects later development of NASH fibrosis after liver transplant

Jiang Li[1], Toshifumi Sato[1], María Hernández-Tejero[1], Juliane I. Beier[1,2], Khaled Sayed[3,4], Panayiotis V. Benos[3], Daniel W. Wilkey[5], Abhinav Humar[6], Michael L. Merchant[5], Andres Duarte-Rojo[7,8] & Gavin E. Arteel[1,2]✉

Although liver transplantation (LT) is an effective therapy for cirrhosis, the risk of post-LT NASH is alarmingly high and is associated with accelerated progression to fibrosis/cirrhosis, cardiovascular disease and decreased survival. Lack of risk stratification strategies hampers early intervention against development of post-LT NASH fibrosis. The liver undergoes significant remodeling during inflammatory injury. During such remodeling, degraded peptide fragments (i.e., 'degradome') of the ECM and other proteins increase in plasma, making it a useful diagnostic/prognostic tool in chronic liver disease. To investigate whether liver injury caused by post-LT NASH would yield a unique degradome profile that is predictive of severe post-LT NASH fibrosis, a retrospective analysis of 22 biobanked samples from the Starzl Transplantation Institute (12 with post-LT NASH after 5 years and 10 without) was performed. Total plasma peptides were isolated and analyzed by 1D-LC–MS/MS analysis using a Proxeon EASY-nLC 1000 UHPLC and nanoelectrospray ionization into an Orbitrap Elite mass spectrometer. Qualitative and quantitative peptide features data were developed from MSn datasets using PEAKS Studio X (v10). LC–MS/MS yielded ~ 2700 identifiable peptide features based on the results from Peaks Studio analysis. Several peptides were significantly altered in patients that later developed fibrosis and heatmap analysis of the top 25 most significantly changed peptides, most of which were ECM-derived, clustered the 2 patient groups well. Supervised modeling of the dataset indicated that a fraction of the total peptide signal (~ 15%) could explain the differences between the groups, indicating a strong potential for representative biomarker selection. A similar degradome profile was observed when the plasma degradome patterns were compared being obesity sensitive (C57Bl6/J) and insensitive (AJ) mouse strains. The plasma degradome profile of post-LT patients yielded stark difference based on later development of post-LT NASH fibrosis. This approach could yield new "fingerprints" that can serve as minimally-invasive biomarkers of negative outcomes post-LT.

Abbreviations

ALT	Alanine aminotransferase
AST	Aspartate aminotransferase
BW	Body weight
CVD	Cardiovascular disease
ECM	Extracellular matrix
GO	Gene ontology
HFD	High fat diet
HOMA-IR	Homeostatic model assessment for insulin resistance

[1]Department of Medicine, University of Pittsburgh, Thomas E. Starzl Biomedical Science Tower, West 1143, 200 Lothrop Street, Pittsburgh, PA 15213, USA. [2]Pittsburgh Liver Research Center, University of Pittsburgh, Pittsburgh, PA, USA. [3]Department of Epidemiology, University of Florida, Gainesville, FL, USA. [4]Present address: Department of Electrical and Computer Engineering and Computer Science, University of New Haven, New Haven, CT, USA. [5]Department of Medicine, University of Louisville, Louisville, KY, USA. [6]Department of Surgery, University of Pittsburgh, Pittsburgh, PA, USA. [7]Division of Gastroenterology and Hepatology, Northwestern Medicine and Feinberg School of Medicine, Northwestern University, Chicago, IL, USA. [8]Comprehensive Transplant Center, Northwestern Medicine and Feinberg School of Medicine, Northwestern University, Chicago, IL, USA. ✉email: gearteel@pitt.edu

KEGG	Kyoto encyclopedia of genes and genomes
LC–MS/MS	Liquid chromatography, tandem mass-spectroscopy
LFD	Low fat diet
Log2FC	Fold-change (log2)
LT	Liver transplantation
MetS	Metabolic syndrome
MMP	Matrix metalloproteinases
MS	Mass spectrometry
NAFLD	Non-alcohol-related fatty liver disease
NASH	Non-alcoholic steatohepatitis
OPLS-DA	Orthogonal partial least squares discriminant analysis

Liver transplantation (LT) is an increasingly utilized therapeutic approach for advanced liver disease. Liver transplantation for from non-alcoholic steatohepatitis (NASH) cirrhosis, is now one of the most common indications for liver transplantation in the US[1,2]. Although LT is an effective therapy for NASH, the risk of post-transplant recurrence is alarmingly high[3,4]; recurrent NASH has an incidence of up to 70% at 5 years, when per protocol biopsies are performed[5]. While the presence of simple steatosis does not appear to impact overall graft and patient survival[3], the presence of NASH is associated with accelerated progression to fibrosis/cirrhosis and cardiovascular disease (CVD), which negatively impact survival[6,7]. Patients that develop de novo NASH, although they have a lower incidence (17% at 5 years), are also at high risk for accelerated progression to NASH fibrosis[5]. Although lifestyle changes and drug therapies are promising approaches to decrease fibrosis related to NASH post-LT and its severe health effects, lack of effective strategies to stratify risk hamper the use of these tools. Moreover, post-LT NASH patients have been excluded from clinical trials testing novel drug therapies for pre-LT NASH. As such, timely risk stratification followed by lifestyle interventions and management of comorbidities will remain as the standard of care in the foreseeable future.

Although there are non-invasive approaches to detect progressing liver fibrosis, including blood-based (e.g., FIB-4) and imaging-based (e.g., stiffness/elastography) assessments, they are less reliable in post-LT patients and their accuracy is suboptimal for the ≤ F2 stage. What is needed is a relatively inexpensive test/score that better stratifies the risk for post-LT NASH fibrosis much earlier in disease progression, where interventive strategies to potentially halt disease progression would be more effective. Moreover, better understanding of drivers of post-LT NASH development could identify new mechanism-based interventive approaches.

The extracellular matrix (ECM) contains a diverse range of components that work bi-directionally with surrounding cells to create a dynamic and responsive microenvironment that regulates cell and tissue homeostasis[8]. Proteases and protease inhibitors contribute to maintaining ECM homeostasis, as well as mediating its changes in response to stress or injury[9,10]. Hepatic fibrosis is a canonical example of ECM dyshomeostasis, leading to accumulation of fibrillary ECM, such as collagen. Although hepatic fibrosis is considered almost synonymous to collagen accumulation[11], the qualitative and quantitative alterations to the hepatic ECM during fibrosis are much more diverse and certainly occur much earlier than fibrotic scarring of the liver[12]. Indeed, transitional changes to the hepatic ECM appear to be key to the normal response to injury[8]. Homeostasis in the ECM is mediated by a balance in the production of ECM, as well as in the degradation of existing ECM by matrix metalloproteinases (MMPs)[13]. Even in cases where there is a net increase in ECM in the liver (e.g., fibrosis) overall turnover is also increased[14]. This group and others have demonstrated that even acute liver injury causes robust changes to the hepatic ECM[15].

The peptidome is defined as the population of low molecular weight biologic peptides (e.g., 0.5–3 kDa), within the cells and biologic fluids. These compartments contain peptides critical for normal organismal function (e.g., peptide hormones and peptide neurotransmitters). The study of the peptidome (i.e., 'peptidomics') is a discipline related to proteomics, but with significant methodological and analytical differences[16]. For example, as the original structure of the peptides is of interest, samples are not trypsin digested prior to mass spectrometry (MS) analysis, as is the case for bottom-up proteomic approaches. This difference originally limited peptide identification, as the available sequence assignment processes were based on trypsin-digested peptide databases; however, the development of de novo sequence assignment methods has addressed this concern[17]. In addition to these naturally-occurring peptides, the peptidome also contains fragments of larger proteins degraded by normal and/or abnormal processes; this family of degraded protein fragments is coined the 'degradome.' This subset of the peptidome has generated great interest in some areas of human health as potential (surrogate) biomarkers for disease; for example, in cancer metastasis, and by extension, in overall patient outcome[17,18].

The purpose of the current study was to identify plasma degradome profile differences in patients that developed post-LT NASH fibrosis to those that did not at an early time-point prior to detectable liver disease (Fig. 1). The results in the human study were also compared to a preclinical model of NAFLD/NASH employing sensitive and insensitive strains of mice to determine if the degradome pattern in humans that develop post-LT NASH fibrosis shows similarity to NASH-sensitive mice (vs. insensitive) in a preclinical mode.

Results

Characterization of the degradome in transplant recipients. Patients were followed for a median of 2 years (range: 1 to 9 years; Fig. 1). Twenty out of 22 (91%) cases had at least one liver biopsy available for review. Post-LT NAFLD was observed among 9 (41%) recipients whereas NASH developed in 6 (27%); 4 were classified as de novo NAFLD/NASH. Progression to at least significant fibrosis (F ≥ 2; "fibrosis") occurred in 12 recipients within 3 years following LT, 4 of whom had underlying post-LT NASH (3 de novo) and one with NAFLD based on a proton-density fat fraction of 29%. When comparing F ≥ 2 "fibrotic" to "non-fibrotic," there were no dif-

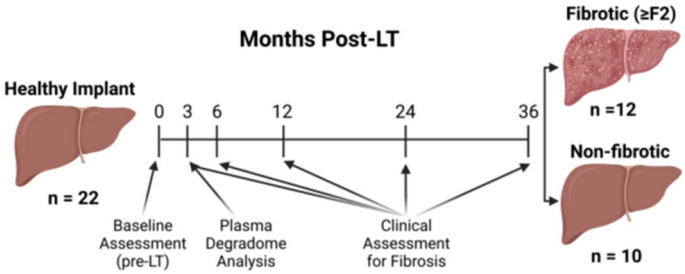

Figure 1. Study design. This was a retrospective analysis that compared 12 post-LT patients (all living donor recipients) that developed significant biopsy-proven NASH fibrosis within 3 years post-LT, to 10 age/sex/weight-matched patients that did not. For the purpose of this study, significant NASH fibrosis was defined as the development of ≥ F2 fibrosis (Brunt-Kleiner score) within 3 years post-LT. LT candidates initially evaluated pre-LT. A blood sample was drawn 3 months after LT along with a clinic visit's laboratories and EDTA plasma was aliquoted and stored at − 80 °C. Samples and relevant deidentified clinical data (e.g., liver chemistry and biopsy results) were collected from recipient 3-, 6- and 12-months post-LT, and annually thereafter. The 3-month sample was analyzed by LC–MS/MS for degradomic profile; using a 3-month "washout" period after LT is standard to remove influences of donor and transplant surgery[3]. Created with Biorender.com.

	Non-fibrotic	fibrotic	P-value
Age	62 ± 7	54 ± 14	0.12
M/F	5/5	6/6	1.0
Etiology	NASH 4 ALD 2 HCV 1 Autoimmune 0 Other 1 Cryptogenic 2	NASH 1 ALD 1 HCV 2 Autoimmune 4 Other 1 Cryptogenic 3	0.16
BMI	30 ± 5	28 ± 5	0.39
Bariatric surgery	0%	8%	0.54

Table 1. Baseline characteristics of LT patients. All assessments were prior to liver transplantation. All transplant recipients were from living donors (LDLT). There were no differences in key baseline characteristics between transplant recipients that developed fibrosis (F ≥ 2 progressors) and those who did not. There were no patients with diabetes mellitus at baseline. Among the group of progressors, 4 recipients (33%) ultimately developed cirrhosis.

ferences in key baseline characteristics before LT (Table 1). Importantly, there were no patients with diabetes mellitus at baseline before LT. Among the group of "fibrosis" patients, 4 recipients (33%) ultimately developed cirrhosis. Allograft rejection, either T-cell- or antibody-mediated occurred on 3 cases (including 2 "fibrotic" with hepatitis C at baseline), none of whom had post-LT NAFLD or NASH.

Analysis of LC–MS/MS data. After LC–MS/MS analysis (see "Methods"), PEAKS was used for visualization of the MS data. Across the two patient groups, 2694 peptides were identified, corresponding to 721 distinct parent proteins (see supplemental Table 3). Of these, a total of 542 peptides (422 in fibrotic and 120 in nonfibrotic), corresponding to 179 distinct proteins, were changed at least twofold between patients who progressed onto ≥ F2 fibrosis ("fibrotic") versus those that did not ("non-fibrotic"). These changes are summarized graphically as a volcano plot (Fig. 2A). Heatmap analysis and hierarchical clustering of top 25 changed peptides of individual patients (Fig. 2B) clustered the "fibrotic" against the "non-fibrotic" well. Supervised orthogonal partial least squares-discriminant analysis (OPLS-DA) score plot of the plasma peptidome profiles of individual patients (Fig. 2C) indicated that a fraction (~ 15%) of the total peptide could explain the differences between the groups.

The parent proteins that contributed to the pattern of significantly changed peptides were analyzed by StringDB[19,20]. This database queries physical and functional protein–protein associations that integrates both experimental and predicted associations. The output creates both graphical and categorical enrichment patterns in the queried dataset. Four key protein family clusters were enriched in the plasma degradome of patients that progressed to at least significant fibrosis (i.e., ≥ F2 staging; "fibrotic"; Fig. 3A), including mitochondrial respiratory chain complex 1 ($p = 1.1 \times 10^{-10}$), tubulin ($p = 7.4 \times 10^{-9}$) collagen chains ($p = 7.7 \times 10^{-7}$) and platelet α-granule ($p = 1.4 \times 10^{-6}$). Similar pathways related to altered metabolism and remodeling were also enriched also in GO (Molecular function) and KEGG analyses (Fig. 3B). GO terms for Cellular Component and Biological Processes provided by StringDB showed similar patterns (supplemental Tables 4 and 5, respectively).

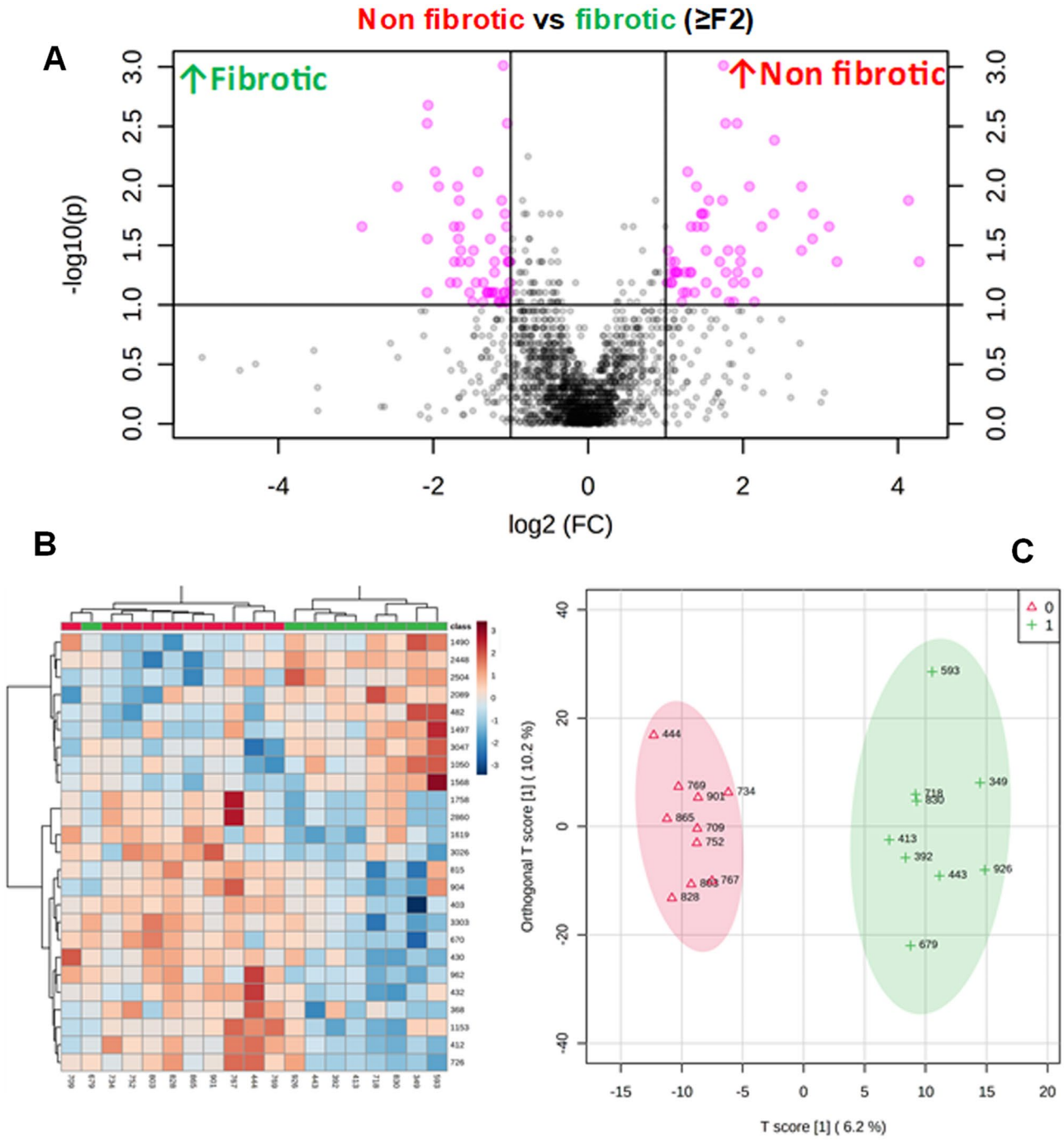

Figure 2. The plasma degradome in post-LT NASH fibrosis. Analysis of the peptidome/degradome in post-LT NASH fibrosis. Summary of analysis of fibrotic (≥ F2; n = 9; green) versus non-fibrotic (n = 10; red) livers of post-LT patients 1 year after LT. (**A**) Volcano plots of changed peptides. (**B**) Heatmap and dendrogram of top 25 changed peptides of individual patients. (**C**) Orthogonal partial least squares-discriminant analysis (OPLS-DA) score plot of the plasma peptidome profiles of individual patients.

Comparing experimental NASH in sensitive and insensitive mice. Although other factors (e.g., immunosuppressive regimens) may also contribute, the primary risk factors for post-LT NASH with fibrosis appear to be synonymous with pre-LT NASH (e.g., obesity, metabolic syndrome and insulin resistance)[21–23]. Although no mouse model completely recapitulates human NAFLD/NASH, dietary manipulation with the obesogenic "Western" diet generates a phenotype similar to that found in human disease in sensitive mouse strains; comparing sensitive versus insensitive mouse strains has been previously used to model human populations at low- versus high-risk for severe NAFLD/NASH[24,25]. Therefore, the concordance of the degradome pattern

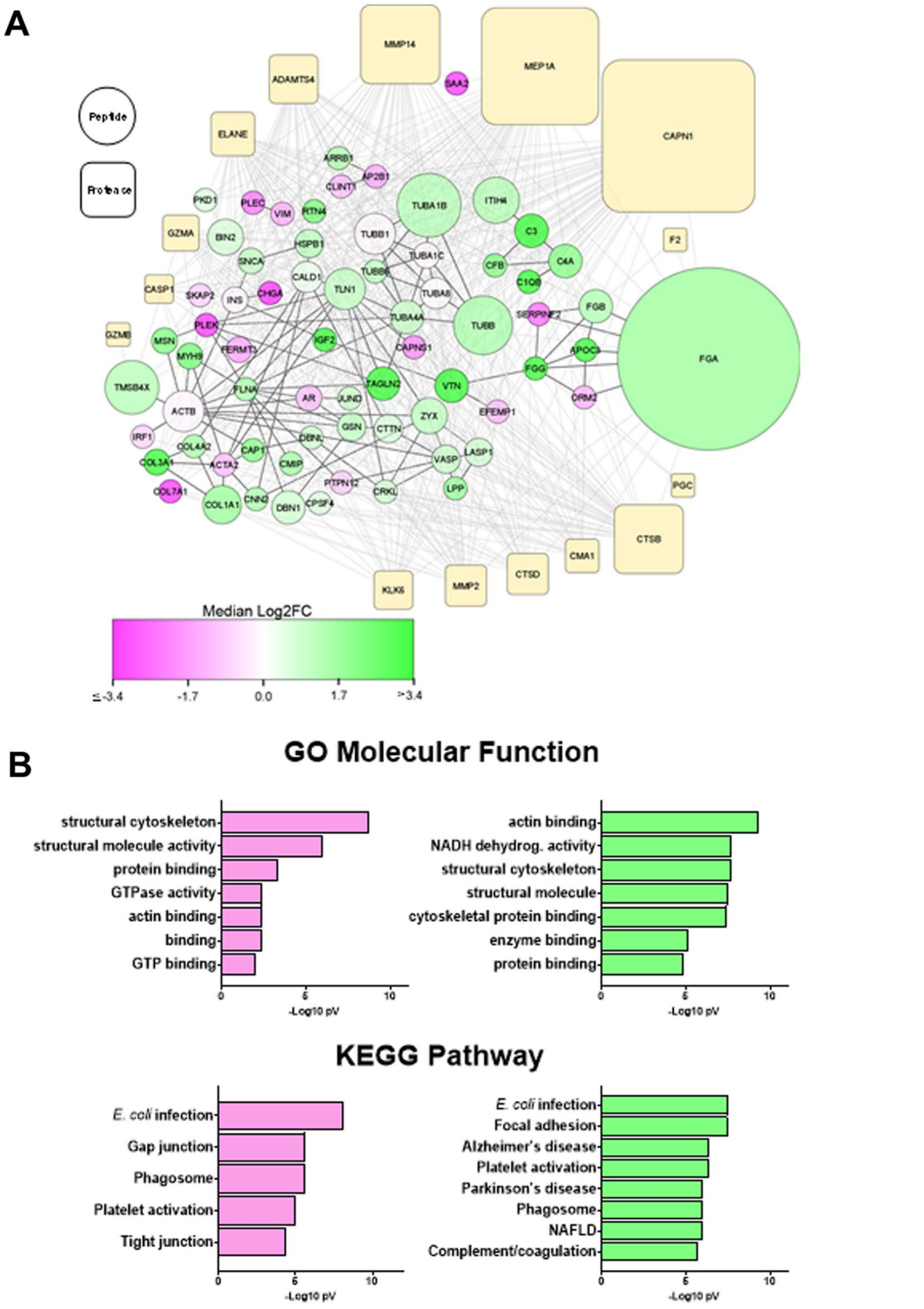

Figure 3. Cluster analysis of the peptidome/degradome in post-LT NASH fibrosis. The peptides significantly increased in NASH fibrosis (see Fig. 1) were analyzed by the Proteasix (http://www.proteasix.org) algorithm using with the positive predictive value (PPV) cut-off to 80%. Protein–protein interaction network analysis of regulated proteomic data sets (q-value < 0.05) was performed using Search Tool for the Retrieval of Interacting Genes/Proteins, STRING v11[20], with the highest confidence score (0.900). The resultant matrix of both Proteasix and STRING analysis were visualized using Cytoscape v3.9.1 (**A**). Node sizes of the predicted proteases represented the relative frequency with which the top 15 proteases were predicted to mediate the observed cleavage (0.2–25%). Node sizes of the peptides represented the relative number of unique peptides (1–56) identified from each parent protein. Node color of the peptides represented the median Log2FC vs non-fibrosers for all peptides derived from that parent protein. Solid lines depict connections between the parent proteins identified by STRING; broken lines depict predicted protease events identified by Proteasix. (**B**) Top GO (molecular functions) and KEGG terms identified cluster/pathway results of STRING analysis for decreased (pink) and increased (green) peptides.

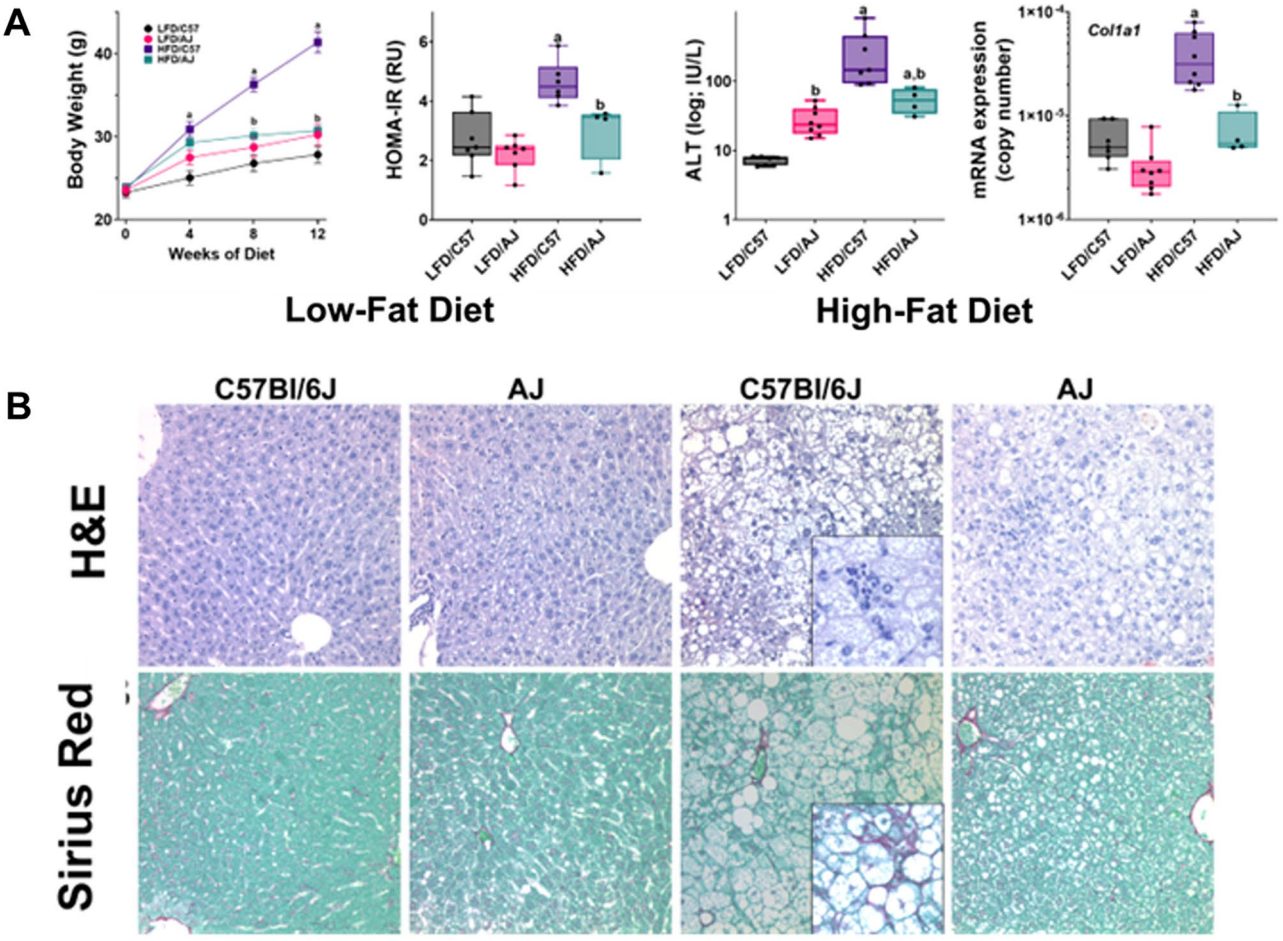

Figure 4. Strain differences in sensitivity to experimental NAFLD/NASH. C57Bl6/J ("C57") and A/J ("AJ") mice were fed the high fat 'Western' ("HFD") or low fat control ("LFD") diet for 12 weeks. The effect of HFD on BW, HOMA-IR plasma ALT (log scale) and expression of Col1A1 (log copy number) was compared (**A**). (**B**) Shows representative photomicrographs of H&E (upper) and Sirius Red (lower) stains. Summary data (**A**) are box and whisker plots (n = 4–8/group), which show the median (thick line), interquartile range (box) and range (whiskers). [a]$P < 0.05$ for effect of HFD, [b]$P < 0.05$ for effect of mouse strain by 2-way ANOVA using Tukey's post hoc test.

between sensitive (i.e., "fibrotic" patients vs. C57Bl6/J mice) and insensitive (i.e., "nonfibrotic" patients vs. AJ mice) was determined.

Accordingly, C57Bl6/J and AJ mice were fed a high fat "Western" diet (HFD) or low fat control diet (LFD) for 12 weeks. As expected, whereas C57Bl6/J mice were sensitive to the obesogenic effects of HFD, AJ mice were relatively insensitive. Specifically, C57Bl6/J mice gained > 70% of their initial body weight (BW) when fed HFD, vs ~ 20% for LFD (Fig. 4A; supplemental Table 6). In contrast, HFD did not significantly alter the rate of BW gain in AJ mice, which was ~ 30% over the course of the study (Fig. 4A). Moreover whereas, HFD increased the homeostatic model assessment for insulin resistance (i.e., HOMA-IR) in C57Bl6/J mice, it did not in AJ mice (Fig. 4A).

Sensitive C57Bl6/J mice also developed significant liver injury when fed a HFD, whereas AJ mice did not. HFD increased liver weight in C57Bl6/J mice by 85%, whereas liver weight did not change in AJ (Supplemental Table 6). HFD also caused severe steatosis, as determined by histological assessment (Fig. 4B) and by biochemical analysis of lipid accumulation (Supplemental Table 6); although moderate macrovesicular steatosis and lipid accumulation was also observed in AJ mice fed HFD (Fig. 4B, Supplemental Table 6), this effect was much less pronounced. The increase in hepatic transaminases caused by HFD (Fig. 4A) was also more severe in C57Bl6/J compared to AJ mice. HFD induced expression of indices of fibrogenesis and collagen accumulation in C57Bl6/J mice (Fig. 4A and Supplemental Fig. 1) and caused the formation of "chicken-wire" fibrosis within the hepatic lobule (Fig. 4B, inset).

Analogous to what was observed in post-LT patients (Fig. 2), HFD dramatically altered the degradome profile in NASH sensitive C57 mice, as compared to the insensitive AJ mice (Fig. 5A). Although unsupervised Principle Component Analysis (PCA) clustered both HFD- and LFD-fed AJ mice together, HFD and LFD feeding clustered the degradome pattern separately for C57BI6/J mice (Fig. 5A). Interestingly, heatmap (Fig. 5C) and OPLS-DA (Fig. 5D) analysis indicated several overlapping 'hits' (e.g., degraded tubulin, fibrinogen and collagen proteins)

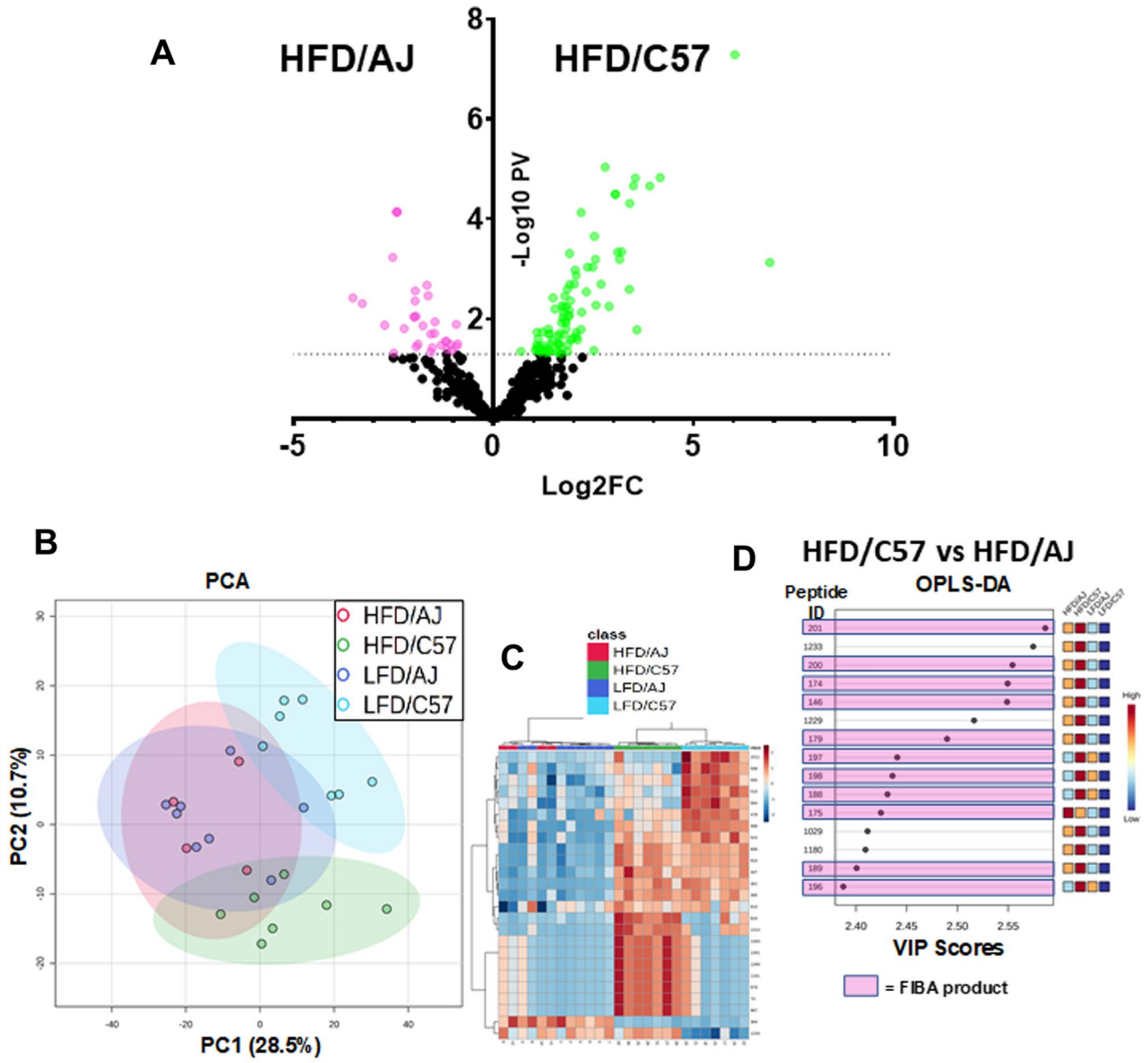

Figure 5. Mouse strain differences in the degradome profile in response to HFD. Feeding conditions are as described in Fig. 4. (**A**) Shows a volcano plot comparing the plasma degradome profile between C57 to AJ mice fed HFD for 12 weeks. (**B**) Shows principal component analysis (PCA) of the degradome profile in AJ and C57 mice fed low- or high fat diets (LFD and HFD). (**C**) shows, heatmap with dendrogram of the top 35 altered peptides. (**D**) shows Variable Importance in Projection (VIP) scores of the top 15 peptides by supervised discriminant analysis (OPLS-DA; see also Fig. 1). Pink highlighted peptides are derived from fibrinogen A (FBA).

as found in the post-LT patients that developed ≥ F2 NASH fibrosis (Fig. 3). Indeed, as in the human data, fibrinogen (FIBA) protein products were dominant in the top scored peptides (Fig. 5D; outlined in pink boxes).

Many proteases cleave substrates with high specificity only at certain sequence sites. Thus, information on the fragment sequence of degraded proteins can inform on proteases that may have generated this pattern. Proteasix (http://www.proteasix.org), an open-source peptide-centric tool to predict in silico the proteases involved in generating these peptides[26]. Figure 3A also shows the relative frequency with which the top 15 proteases were predicted to generate the resultant degradome peptides by this analysis. Figure 6A shows a frequency distribution figure comparing the degradome in humans that progressed to ≥ F2 after LT versus sensitive mice (C57Bl6/J) fed a high fat diet. The two top predicted proteases, Calpain -1/-2 (Capn1/2) and Meprin-1a (Mep1a) were shared between the species under these conditions (Figs. 2A and 6A). The expression of the splice variants of Capn1/2 (*Capn1* and *Capn1*) was determined via real-time rtPCR in mouse liver (Fig. 6B). Both isoform variants were expressed in liver, with *Capn2* expression being more abundant. HFD feeding significantly induced expression of these splice variants in the C57Bl6/J strain fed HFD (vs. AJ mice; Fig. 6B). A similar effect was observed for *Mep1a* expression (Fig. 6B). Several of the predicted CAPN1/2 and MEP1A substrates for these enzymes

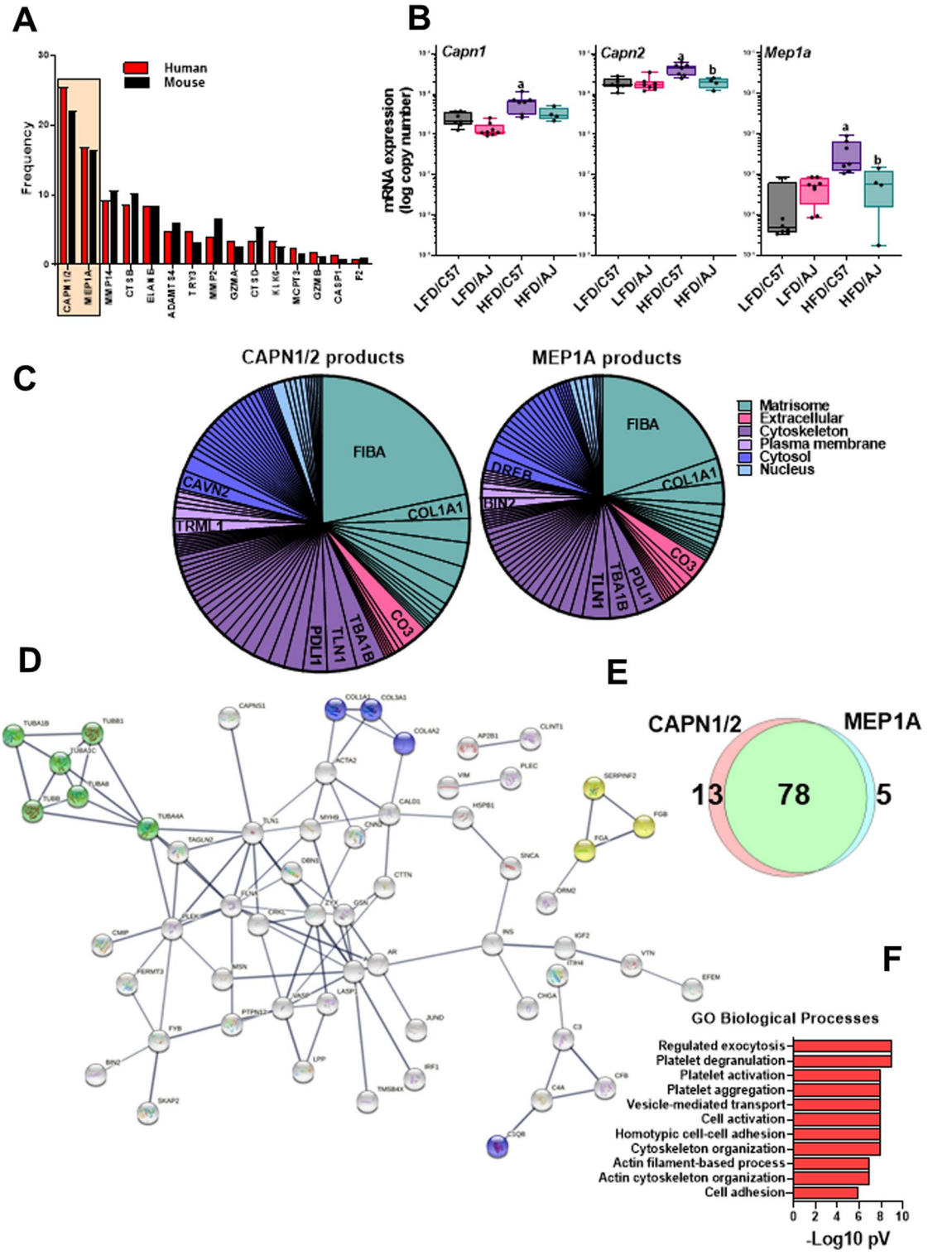

Figure 6. The plasma degradome predicts hepatic protease induction in both human pre-LT NASH fibrosis and experimental mouse NAFLD/NASH. (**A**) shows the top 15 proteases by predicted Proteasix analysis in post-LT NASH fibrosis (red) and in experimental NAFLD/NASH (C57 HFD vs AJ HFD; see Fig. 4; black). The expression of the top predicted proteases (CAPN1/2 and MEP1A) was determined in liver samples from C57 and AJ mice (**B**) by qPCR. The predicted substrates (**C**) and GO Biological Process of these predicted substrates in the human samples (**D**) are also shown. (**E**) shows a Venn diagram depicting the overlap of predicted substrates for CAPN1/2 and MEP1A and (**D**) shows top-ranked GO terms for Biological Processes associated with this enrichment pattern. Summary data (**B**) are box and whisker plots (n = 4–8/group), which show the median (thick line), interquartile range (box) and range (whiskers). [a]$P < 0.05$ for effect of HFD, [b]$P < 0.05$ for effect of mouse strain by 2-way ANOVA using Tukey's post hoc test.

(Fig. 6C,E) were analogous to the key nodes identified by StringDB analysis for the degradome as a whole (Fig. 3A) and the enriched GO Biological Processes of these substrates related to remodeling and coagulation cascade activation (Fig. 6F).

CausalMGM, a probabilistic graph modeling algorithm, was employed to analyze the degradome data enriched in humans that went on to develop post-LT NASH fibrosis (i.e., "fibrotic"; this algorithm predicts direct associations among and between degradome features, as well as clinical data. The resulted graph encodes variables as nodes and direct connections between variables as (directed) edges. The first and second neighbors of the post-LT NASH fibrosis variable (i.e., "fibrotic") are presented in Fig. 7A. The most informative variables for predicting the development of post-LT NASH fibrosis are those in its Markov blanket (Fig. 7A, circles): TYB4, VINC, FIBA, and NEUG. Besides Sex, no other clinical variable was found to be in the proximity predicting the development of ≥ F2 fibrosis. Figure 7B shows the frequency distribution of the predicted proteases profiles for identified first- and second-degree neighbors in the Markov blanket identified by CausalMGM. In this subset of peptides, Capn1 and Mep1a were again the most predicted proteases, similar to the degradome in toto for both humans and mice (see Figs. 2 and 6), although Mep1a was slightly enriched compared to those analyses.

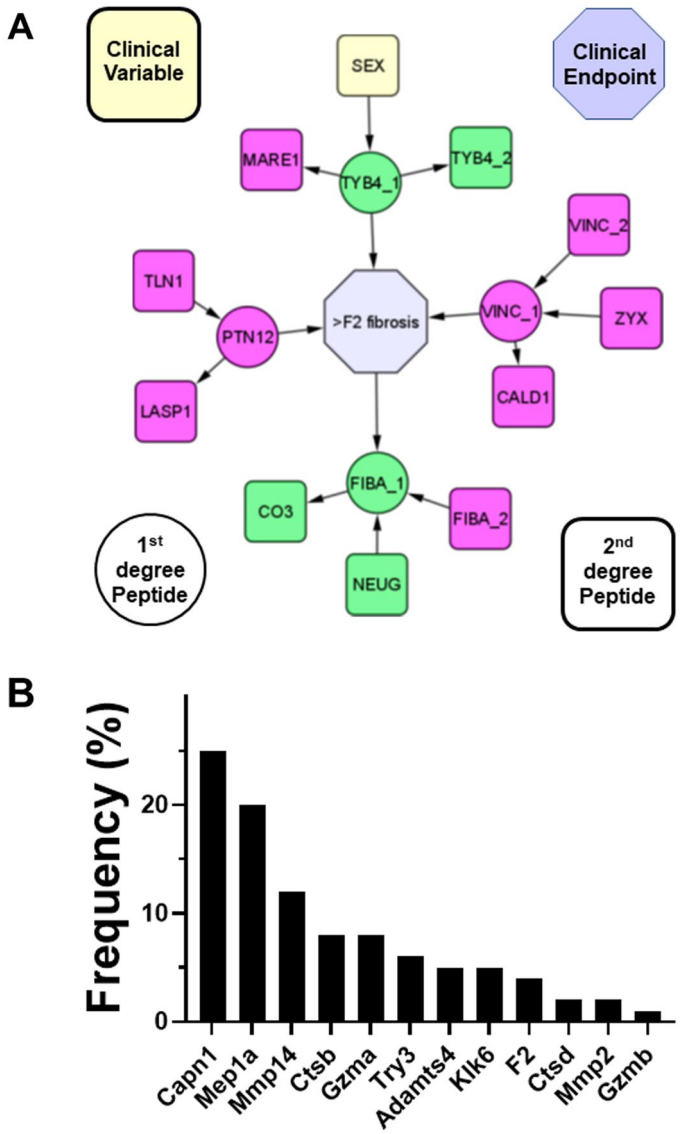

Figure 7. Probabilistic graphical modeling of predictive peptides. (**A**) Shows the probabilistic graph around the variable representing post-LT NASH fibrosis (≥ F2). Only the first and second neighbors of F2 are depicted. The input dataset included all peptidome features and demographic and clinical variables. Based on this graph, the most informative variables for F2 are those in its Markov blanket (yellow nodes). (**B**) shows frequency distribution of predicted proteases derived from the 1st and 2nd degree neighbors determined by probabilistic graphical modeling (**A**). Colored nodes indicate fold-change of the peptides versus non-fibrosing controls (green increased, cyan decreased).

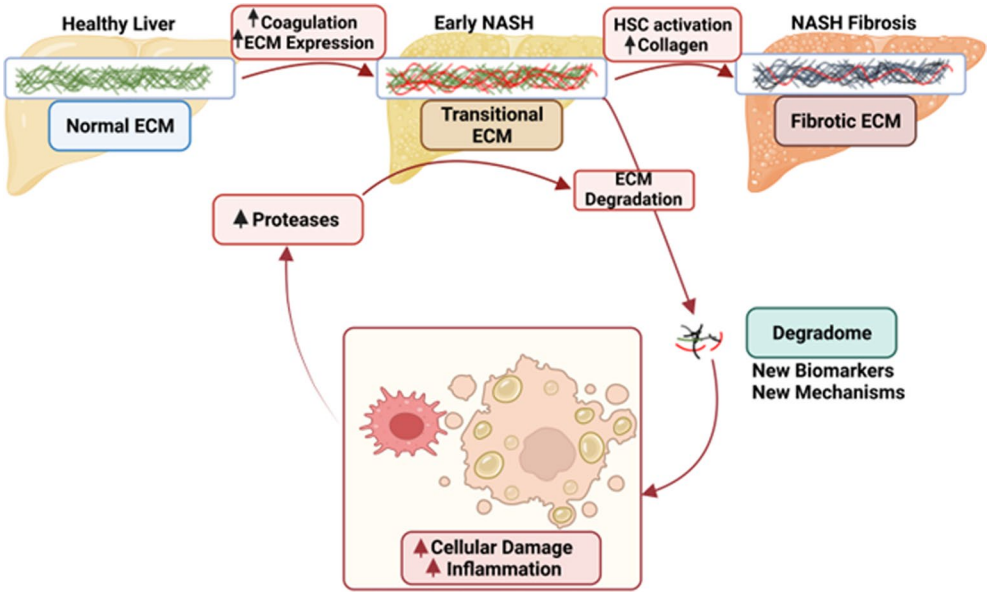

Figure 8. Working hypothesis. Acute injury causes formation of a transitional ECM. This transitional ECM may contribute to injury and inflammation. The transitional ECM often resolves after removal of the insult and may contribute to the recovery from that insult. With continued injury, the transitional matrix may progress to a fibrotic matrix, which can also resolve under some conditions. Even during ECM accumulation in response to acute/chronic injury, there is a net increase in turnover of the matrisome, yielding degraded ECM products. It is hypothesized that qualitative and quantitative changes to the "degradome" will serve as a biomarkers for outcome and mechanism in post-LT NASH fibrosis. Created with Biorender.com.

Discussion

As mentioned in the Introduction, there is a critical need for non-invasive approaches that accurately predict the risk of the development post-LT NASH fibrosis earlier in disease progression. Hypothesis-driven approaches are key to elucidating mechanism. However, the nature of these approaches requires prior knowledge. Most research to date on NASH fibrosis development has focused on key collagenous ECM proteins identified histologically to be involved in fibrogenesis. In contrast, it is understood that remodeling of an organ is an orchestrated response not necessarily restricted to end-stage fibrosis, collagens or even ECM proteins (Fig. 8). Discovery-based 'omic techniques coupled with informatic analyses can yield new information and insight into disease progression and regression. In addition to synthesized peptides, the peptidome also contains fragments of proteins degraded by normal and/or abnormal processes (i.e., 'degradome') and shed into the surrounding biofluid space (Fig. 8). Given the increased protein turnover associated with hepatic remodeling and disease, it was hypothesized that the degradome may serve as a new prognostic tool (Fig. 8). These degradomic profiles are conditionally unique to the metabolic/pathologic status of the organism and reflect not only quantitative changes (i.e., more/less parent protein to degrade), but also qualitative changes (i.e., change in the pattern of protease digestion of parent proteins).

When the degradome was analyzed, an interesting pattern resolved. Specifically, there were distinct and significant differences in the pattern of the degradome in plasma from patients that later went on to develop at least significant (i.e., ≥ F2) post-LT NASH fibrosis and those that did not (Fig. 2). Unsupervised (heatmap and dendrogram) hierarchical clustering was able to separate the 2 groups well (Fig. 2B). Moreover, supervised (OPLS-DA) discriminant analysis indicated that a fraction of the total peptide signal likely drives the assumed difference between the groups (Fig. 2C). These data suggest that the degradome pattern is differential in those that latter develop fibrosis 3 months after LT, which is well before fibrosis was detectable with clinical assessment.

Degradomic analysis allows for the integration of both quantitative (i.e., more/less parent protein degraded) and qualitative (i.e., change in the pattern of protease digestion of parent proteins) changes in the analysis (Fig. 3). Increases the amount and number of ECM fragments previously associated with fibrosis development (e.g., collagens; Fig. 3) was observed[27]. However, one of the most robust family of degraded proteins that was enriched in "fibrotic" were associated with the coagulation cascade, with a particular enrichment of the fibrin(ogens) (e.g., FGA; Fig. 3; supplemental Table 3). Supervised discriminant analysis and machine learning approaches also ranked FGA peptides as important to predict post-LT NASH fibrosis development in human samples (Figs. 2 and 7). Moreover, a similar enrichment of FGA fragments was observed when NASH-sensitive (C57Bl6/J) and -insensitive (AJ) mouse strains were compared (Fig. 5).

Although previous studies have investigated the potential role of fibrin(ogens) in the development of hepatic injury and fibrosis, the results are somewhat conflicting[28,29]. In contrast, the turnover of fibrin(ogen) ECM has been heavily studied in other diseases of remodeling. For example, fibrin(ogen) ECM plays a key role in subcutaneous wound-healing[30]. Indeed, recent work suggests that fibrin clot turnover (i.e., fibrinolysis) may be key in driving hepatic fibrosis development, versus fibrin(ogen) ECM accumulation, per se[31]. Here, fragments of fibrino(ogen) were dominant features of the degradome in patients that progressed to severe post-LT NASH

fibrosis, as well in a preclinical animal model; several of these fragments were also predicted informatically to drive phenotype. Since hepatic fibrosis and subcutaneous wound-healing qualitatively and quantitatively share many similarities, it is possible this this increase in fibrin(ogen) fragments represents an early detectable transition from provisional ECM to a collagenous ECM (Fig. 8). Future studies should specifically investigate this possibility, especially given the use of anticoagulants in fibrotic liver disease and cirrhosis.

As mentioned in the Introduction, collagenous ECM accumulation has been the major focus in the field of hepatic fibrosis[15]. Likewise, proteases involved in resolution of collagenous ECM (e.g., MMP2 and MMP9) have also received a sizeable amount of attention[32]. The fragment sequence and putative cleavage site of the degradome may yield new information on proteases involved. The predicted protease that generated each peptide was therefore determined by in silico analysis of the cleavage site using the online open-source tool, Proteasix (http://www.proteasix.org; Fig. 3)[26]. Although several proteases with established roles in fibrosis and/or resolution were identified (e.g., MMP2; Fig. 3), several novel players were predicted by the algorithm. The most common predicted proteases in both humans and in our preclinical animal model were Capn1/2 and Mep1A (Figs. 3 and 6). It should be noted that Capn1 and its isozyme Capn2 cannot be delineated by substrate or activity assays, and expression of both followed a similar pattern in liver during fibrosis in our preclinical model (Fig. 6B). Moreover, there is significant overlap between Capn1/2 and Mep1a in predicted substrate targets (Fig. 6C–E). Capn1/2 and Mep1a are both cysteine proteases that cleave a myriad of protein substrates. Although they are generally localized intracellularly or on the plasma membrane, they can also be excreted in the active state[33]. Capn1/2 and Mep1a activation has been identified as a key driver of inflammation in other diseases of inflammation and remodeling, such as atherosclerosis and cardiac disease[33–36]. Interestingly, the predicted substrates for Capn1/2 and/or Mep1a activation not only included key ECM proteins [e.g., collagens and fibrin(ogens)], but also nuclear proteins, such as histones (Fig. 6C). Few studies have investigated these proteases in hepatic injury[37]. Moreover, recent work by this group showed that Capn2 is progressively induced in pretransplant NASH fibrosis severity[38]. The mechanisms by which Capn2 may mediate these effects are unclear but work in other organ systems suggest a role in not only ECM metabolism, but also in organelle damage [e.g.,[33–36]]. These data suggest that the role of Capn1/2 and Mep1a in liver disease and fibrosis may be underappreciated at this time.

In conclusion, the identification of critical cleavage points of proteins is a novel and cutting-edge approach in the liver diseases field. The present study demonstrates the utility of degradomic approaches for development of novel biomarkers. The degradome characterization could lead to a better understanding of the specific pathological processes that trigger and perpetuate abnormal ECM remodeling that result in fibrosis and cirrhosis. Degradomic peptide patterns may also play a role in predicting early liver fibrosis onset in the setting of post-LT NAFLD/NASH and, consequently, LT outcomes.

LT patients are generally strongly committed to their continued treatment and are more heavily monitored than other patient cohorts (e.g., pre-LT NASH fibrosis); therefore, dropout rates in this group tend to be very low (< 5%). Moreover, non-invasive assessment of post-LT fibrosis is per protocol in most transplant centers. Nevertheless, a limitation of this study is that there is a risk of selection bias for patients for whom follow-up analyses of liver disease were performed. Moreover, it is unclear if the results observed here are more broadly translatable to fibrosis development, such as pre-LT NASH fibrosis. If true, the identified protein products could become potentially targetable molecules to develop new therapies against the progression of liver fibrosis, regardless of etiology. Further prospective and etiology-controlled studies are needed to confirm and potentially expand these results.

Methods

Biobanked patient samples. This was a retrospective analysis that compared 12 post-LT patients (all living donor recipients) that developed significant biopsy-proven NASH fibrosis within 3 years post-LT, to 10 age/sex/weight-matched patients that did not (see Table 1 and Fig. 1). The study was approved by The University of Pittsburgh Medical Center/University of Pittsburgh (UPMC/Pitt) institutional IRB committee. Informed consent was waived due to the retrospective nature of the study by UPMC/Pitt institutional IRB. For the purpose of this study, significant NASH fibrosis was defined as the development of ≥ F2 fibrosis (Brunt-Kleiner score) within 3 years post-LT. According to an institutional research protocol, LT candidates were approached by the time of evaluation (i.e., pre-LT) by research coordinators and asked to participate in UPMC LT Biobanking Protocol. Following consent, a blood sample was drawn 3 months after LT along with a clinic visit's laboratories and EDTA plasma was aliquoted and stored at − 80 °C. Those candidates successfully achieving transplantation continued to participate in the post-LT period contributing with specimens for biobanking. Samples and relevant deidentified clinical data (e.g., liver chemistry and biopsy results) were collected from recipient 3-, 6- and 12-months post-LT, and annually thereafter. The 3-month sample was analyzed by LC–MS/MS for degradomic profile (see below); using a 3-month "washout" period after LT is standard to remove influences of donor and transplant surgery[3].

Clinical endpoints. De-identified post-LT records were obtained through an honest broker. Per protocol, the transplant program performs allograft biopsies and liver imaging at 1 year after living donor LT, which are mandated in addition to clinically-indicated investigations. Imaging-based non-invasive liver disease assessment is also obtained on a yearly basis, including magnetic resonance elastography and proton-derived fat fraction. Post-LT NAFLD was defined as steatosis ≥ 5% on liver biopsy or as a proton-density fat fraction ≥ 6.4%, whereas NASH was defined as the presence of steatosis plus steatohepatitis or a perivenular pattern of fibrosis suggestive of NASH per pathology reports. The primary endpoint from our clinical cohort was progression to at least significant fibrosis (F ≥ 2), defined on the basis of liver biopsy, magnetic resonance elastography ≥ 3.1 kPa or obvious imaging features of cirrhosis plus incidental features and clinical complications from portal hyperten-

sion (splenomegaly excluded). For recurrent cirrhosis, a threshold of 4.7 kPa was utilized for magnetic resonance elastography.

Animals and treatments. All animals were housed in a pathogen-free barrier facility accredited by the Association for Assessment and Accreditation of Laboratory Animal Care, and procedures were approved by the University of Pittsburgh Institutional Animal Care and Use Committee (IACUC). All experiments were performed in accordance with guidelines and regulations of University of Pittsburgh and ARRIVE guidelines (https://arriveguidelines.org). Previous studies have indicated that there are strain differences in mice in the sensitivity of the liver to damage caused by an obesogenic diet[39]. Specifically, although AJ and C57Bl/6J mice both develop insulin resistance when fed HFD, the latter strain develops much more robust liver disease[24,25,40,41]. Accordingly, 8 weeks old, male AJ and C57Bl/6J mice purchased from Jackson Laboratory (Bar Harbor, ME) and animals were allowed standard laboratory chow and water ad libitum. Mice were fed either a low fat control diet (LFD: 13% saturated fat) or a 'Western'-style high fat, high-fructose diet (HFD: 42% saturated fat) for 12 weeks as described previously[42,43]. Animals were weighed on a weekly basis to check growth and food consumption was monitored. Mice were fasted for 4 h prior to sacrifice. At the time of sacrifice, animals were anesthetized with ketamine/xylazine (100/15 mg/kg, i.p.). Blood was collected from the vena cava just prior to sacrifice by exsanguination and citrated plasma was stored at − 80 °C for further analysis. Portions of liver tissue were frozen immediately in liquid nitrogen, while others were fixed in 10% neutral buffered formalin or embedded in frozen specimen medium (Tissue-Tek OCT compound, Sakura Finetek, Torrance, CA) for subsequent sectioning and mounting on microscope slides.

RNA isolation and real-time RT-PCR. RNA extraction and real-time RT-PCR were performed as described previously[43]. RNA was extracted immediately following sacrifice from fresh liver samples using RNA Stat60 (Tel-Test, Ambion, Austin, TX) and chloroform. RNA concentrations were determined spectrophotometrically and 1 µg of total RNA was reverse transcribed using the QuantiTect Reverse Transcription Kit (Qiagen,Valencia, CA). Real-time RT-PCR was performed using a StepOne real time PCR system (Thermo Fisher Scientific, Grand Island, NY) using the Taqman Universal PCR Master Mix (Life Technologies, Carlsbad, CA). Primers and probes were ordered as commercially available kits (Thermo Fisher Scientific, Grand Island, NY; see Supplemental Table 1). The comparative C_T method was used to determine fold differences between the target genes and an endogenous reference gene (*18s*). Results were reported as copy number ($2^{-\Delta CT}$) versus *18s*.

Biochemical assays and histology. Plasma levels of Aspartate transaminase (AST) and alanine amino transferase (ALT) were determined spectrophotometrically using standard kits (Thermo Fisher Scientific, Waltham, MA), as described previously[44]. Formalin-fixed, paraffin embedded sections were cut at 5 µm and mounted on glass slides. Deparaffinized sections stained with hematoxylin and eosin and pathology were assessed in a blinded manner. ECM accumulation in liver sections was determined by staining with Sirius red/fast green and were visualized via brightfield analysis[45].

Plasma peptide purification and high resolution LC–MS/MS analysis. 1 volume of PBS and 0.025 volumes of 10X iRT standards (Biognosis Inc, Beverly, MA) were added to 1 volume of plasma. 20% w/v TCA was mixed into each sample on ice to a final concentration of 10% w/v. Samples were then incubated for 1 h at 4 °C. The precipitate was pelleted by centrifugation at 16,000 × G for 10 min at 4 °C; pellets were discarded. The centrifugation was then repeated with the supernatant samples, followed by discard of the second pellets. Samples were then desalted and concentrated using solid phase extraction (Waters Oasis HLB µElution 30 µm plate, part no. 186001828BA) as described[46,47]. Solid phase extraction eluates were dried in a SpeedVac, and dried peptides were re-suspended in 2% v/v acetonitrile/ 0.1% v/v formic acid to yield an iRT concentration of 1X (assuming complete recovery). 1 µL of each sample was separated using an Acclaim PepMap 100 75 µm × 2 cm, nanoViper (C18, 3 µm, 100 Å) trap, and an Acclaim PepMap RSLC 50 µm × 15 cm, nanoViper (C18, 2 µm, 100 Å) separating column (ThermoFisher Scientific, Waltham, MA, USA) for mouse degradome samples or an Acclaim PepMap RSLC 75 µm × 50 cm, nanoViper (C18, 2 µm, 100 Å) separating column (ThermoFisher) for human degradome samples. Peptides were eluted under a 60 min 2–37% acetonitrile gradient for mouse degradome (2%-45% for human degradome) and transferred by Nanospray Flex nanoelectrospray source (ThermoFisher) into an Orbitrap Elite—ETD mass spectrometer (ThermoFisher) using an Nth Order Double Play (Xcalibur v2.2, ThermoFisher) with FTMS MS1 scans (240,000 resolution) collected from 300 to 2000 m/z and ITMS MS2 scans collected on up to twenty peaks having a minimum signal threshold of 5000 counts from the MS1 scan event.

Peptidomic data analysis. RAW files were searched in Peaks Studio X (Bioinformatics Solutions Inc., Waterloo, ON, Canada) using the Denovo, PeaksDB, PeaksPTM, and Label Free Q algorithms. The UniprotKB reviewed reference proteome canonical and isoform Homo sapiens sequences (Proteome ID UP000005640) version 11/30/2020 was used for the human degradome samples and the Mus musculus sequences (Proteome ID UP000000589) version 7/22/2021 for the mouse degradome samples. Search parameters included: variable methionine and proline oxidation (+ 15.9949 Da), no enzyme specified, 15 ppm precursor error for MS1 Orbitrap FTMS data, 0.5 Da error for MS2 data sets, and selected common PTMs in the PeaksPTM algorithm. The peptide, feature, and protein-peptide csv files were exported from the Label Free Q result for statistical tests in Microsoft Excel 2016 and R v3.5.0. High confidence peptide assignments (Peaks Studio X criteria –logP scores with FDR threshold 1%) were exported into comma separated values files (.csv) for upload and analysis by the Proteasix (http://www.proteasix.org) algorithm using the 'Peptide-centric' prediction tool based on curated,

known and observed cleavage events enabling assignment of protease identities from the MEROPS database as described previously[48]. The positive predictive value (PPV) cut-off for the prediction algorithm output was set to 80%. Protein–protein interaction network analysis of regulated proteomic data sets (q-value < 0.05) was performed using Search Tool for the Retrieval of Interacting Genes/Proteins, STRING v11[20], with the highest confidence score (0.900). The resultant matrix of both Proteasix and STRING analysis were visualized using Cytoscape v3.9.1. Node sizes of the predicted proteases represented the relative frequency with which the top 15 proteases were predicted to mediate the observed cleavage (0.2–27%). Node sizes of the peptides represented the relative number of unique peptides (1–56) identified from each parent protein. Node color of the peptides represented the median Log2FC vs non-fibrosers for all peptides derived from that parent protein.

Probabilistic graphical modeling. The peptidomic data were normalized using nonparanormal (npn) transformation[49], and combined the normalized data with clinical variables including sex, age, fibrosis stage (F2–F4), NAFLD/NASH diagnosis, rejection and years follow-up to create a data matrix with mixed data types. CausalMGM[50], with the Fast Greedy Equivalence Search (FGES) algorithm (penalty discount = 6) was employed to construct a probabilistic graph and identify variables in the Markov blanket of F2 fibrosis.

Data sharing. Proteomic files were deposited in MassIVE (http://massive.ucsd.edu/) under a study entitled "Post-liver transplant plasma degradome reflects later development of severe NASH fibrosis". Data included (A) the primary data files (.RAW), (B) peak list files (.mzML), (C) sample key, (D) the sequence databases (mouse and human UniprotKB reviewed reference proteoms), and (E) excel files containing Peaksdb results for de novo peptide sequence assignment. Shared data were be released from private embargo for public access upon acceptance for publication.

Data availability

Proteomic files were deposited in MassIVE (http://massive.ucsd.edu/) under a study entitled "Post-liver transplant plasma degradome reflects later development of severe NASH fibrosis". Data include (A) the primary data files (.RAW), (B) peak list files (.mzML), (C) sample key, (D) the sequence databases (mouse and human UniprotKB reviewed reference proteoms), and (E) excel files containing Peaksdb results for de novo peptide sequence assignment. Shared data were be released from private embargo for public access upon acceptance for publication. All other data will be made available on request.

Received: 14 February 2023; Accepted: 13 June 2023
Published online: 20 June 2023

References

1. Shirazi, F., Wang, J. & Wong, R. J. Nonalcoholic steatohepatitis becomes the leading indication for liver transplant registrants among US adults born between 1945 and 1965. *J. Clin. Exp. Hepatol.* **10**, 30–36. https://doi.org/10.1016/j.jceh.2019.06.007 (2020).
2. Cotter, T. G. & Charlton, M. Nonalcoholic steatohepatitis after liver transplantation. *Liver Transpl.* **26**, 141–159. https://doi.org/10.1002/lt.25657 (2020).
3. Narayanan, P. *et al.* Recurrent or de novo allograft steatosis and long-term outcomes after liver transplantation. *Transplantation* **103**, e14–e21. https://doi.org/10.1097/TP.0000000000002317 (2019).
4. Taneja, S. & Roy, A. Nonalcoholic steatohepatitis recurrence after liver transplant. *Transl. Gastroenterol. Hepatol.* **5**, 24. https://doi.org/10.21037/tgh.2019.10.12 (2020).
5. Vallin, M. *et al.* Recurrent or de novo nonalcoholic fatty liver disease after liver transplantation: Natural history based on liver biopsy analysis. *Liver Transpl.* **20**, 1064–1071. https://doi.org/10.1002/lt.23936 (2014).
6. Gitto, S. *et al.* Nonalcoholic steatohepatitis before and after liver transplant: Keeping up with the times. *Expert Rev. Gastroenterol. Hepatol.* **13**, 173–178. https://doi.org/10.1080/17474124.2019.1551132 (2019).
7. Saeed, N. *et al.* Incidence and risks for nonalcoholic fatty liver disease and steatohepatitis post-liver transplant: Systematic review and meta-analysis. *Transplantation* **103**, e345–e354. https://doi.org/10.1097/TP.0000000000002916 (2019).
8. Poole, L. G. & Arteel, G. E. Transitional remodeling of the hepatic extracellular matrix in alcohol-induced liver injury. *Biomed. Res. Int.* **2016**, 3162670. https://doi.org/10.1155/2016/3162670 (2016).
9. Lu, P., Takai, K., Weaver, V. M. & Werb, Z. Extracellular matrix degradation and remodeling in development and disease. *Cold Spring Harb. Perspect. Biol.* https://doi.org/10.1101/cshperspect.a005058 (2011).
10. Hynes, R. O. The extracellular matrix: Not just pretty fibrils. *Science* **326**, 1216–1219 (2009).
11. Friedman, S. L. Stellate cell activation in alcoholic fibrosis—An overview. *Alcohol Clin. Exp. Res.* **23**, 904–910. https://doi.org/10.1111/j.1530-0277.1999.tb04201.x (1999).
12. Gressner, O. A., Weiskirchen, R. & Gressner, A. M. Evolving concepts of liver fibrogenesis provide new diagnostic and therapeutic options. *Comp. Hepatol.* **6**, 7. https://doi.org/10.1186/1476-5926-6-7 (2007).
13. Campana, L. & Iredale, J. P. Regression of liver fibrosis. *Semin. Liver Dis.* **37**, 1–10. https://doi.org/10.1055/s-0036-1597816 (2017).
14. Roderfeld, M. Matrix metalloproteinase functions in hepatic injury and fibrosis. *Matrix Biol.* **68–69**, 452–462. https://doi.org/10.1016/j.matbio.2017.11.011 (2018).
15. Arteel, G. E. & Naba, A. The liver matrisome—Looking beyond collagens. *JHEP Rep. Innov. Hepatol.* **2**, 100115. https://doi.org/10.1016/j.jhepr.2020.100115 (2020).
16. Schrader, M., Schulz-Knappe, P. & Fricker, L. D. Historical perspective of peptidomics. *EuPA Open Proteom.* **3**, 171–182. https://doi.org/10.1016/j.euprot.2014.02.014 (2014).
17. Greening, D. W., Kapp, E. A. & Simpson, R. J. The peptidome comes of age: Mass spectrometry-based characterization of the circulating cancer peptidome. *Enzymes* **42**, 27–64. https://doi.org/10.1016/bs.enz.2017.08.003 (2017).
18. Lai, Z. W., Petrera, A. & Schilling, O. The emerging role of the peptidome in biomarker discovery and degradome profiling. *Biol. Chem.* **396**, 185–192. https://doi.org/10.1515/hsz-2014-0207 (2015).
19. Szklarczyk, D. *et al.* STRING v11: Protein-protein association networks with increased coverage, supporting functional discovery in genome-wide experimental datasets. *Nucleic Acids Res.* **47**, D607–D613. https://doi.org/10.1093/nar/gky1131 (2019).
20. Szklarczyk, D. *et al.* The STRING database in 2021: Customizable protein-protein networks, and functional characterization of user-uploaded gene/measurement sets. *Nucleic Acids Res.* **49**, D605-d612. https://doi.org/10.1093/nar/gkaa1074 (2021).

21. Pais, R. *et al.* NAFLD and liver transplantation: Current burden and expected challenges. *J. Hepatol.* **65**, 1245–1257. https://doi.org/10.1016/j.jhep.2016.07.033 (2016).
22. Germani, G. *et al.* Management of recurrent and de novo NAFLD/NASH after liver transplantation. *Transplantation* **103**, 57–67. https://doi.org/10.1097/TP.0000000000002485 (2019).
23. Kappus, M. & Abdelmalek, M. D. Novo and recurrence of nonalcoholic steatohepatitis after liver transplantation. *Clin. Liver Dis.* **21**, 321–335. https://doi.org/10.1016/j.cld.2016.12.006 (2017).
24. Kondo, H. *et al.* Differential regulation of intestinal lipid metabolism-related genes in obesity-resistant A/J vs. obesity-prone C57BL/6J mice. *Am. J. Physiol. Endocrinol. Metab.* **291**, e1092–e1099. https://doi.org/10.1152/ajpendo.00583.2005 (2006).
25. Rogers, A. B. Stress of strains: Inbred mice in liver research. *Gene Expr.* **19**, 61–67. https://doi.org/10.3727/105221618X15337408678723 (2018).
26. Klein, J. *et al.* Proteasix: A tool for automated and large-scale prediction of proteases involved in naturally occurring peptide generation. *Proteomics* **13**, 1077–1082. https://doi.org/10.1002/pmic.201200493 (2013).
27. Schuppan, D., Ruehl, M., Somasundaram, R. & Hahn, E. G. Matrix as a modulator of hepatic fibrogenesis. *Semin. Liver Dis.* **21**, 351–372. https://doi.org/10.1055/s-2001-17556 (2001).
28. Lee, K. C. *et al.* Dabigatran reduces liver fibrosis in thioacetamide-injured rats. *Dig. Dis. Sci.* **64**, 102–112. https://doi.org/10.1007/s10620-018-5311-1 (2019).
29. Beier, J. I. *et al.* Fibrin accumulation plays a critical role in the sensitization to lipopolysaccharide-induced liver injury caused by ethanol in mice. *Hepatology* **49**, 1545–1553. https://doi.org/10.1002/hep.22847 (2009).
30. Kearney, K. J., Ariëns, R. A. S. & Macrae, F. L. The role of fibrin(ogen) in wound healing and infection control. *Semin. Thromb. Hemost.* https://doi.org/10.1055/s-0041-1732467 (2021).
31. Kopec, A. K. & Luyendyk, J. P. Role of fibrin(ogen) in progression of liver disease: Guilt by association?. *Semin. Thromb. Hemost.* **42**, 397–407. https://doi.org/10.1055/s-0036-1579655 (2016).
32. Friedman, S. L. & Pinzani, M. Hepatic fibrosis 2022: Unmet needs and a blueprint for the future. *Hepatology* https://doi.org/10.1002/hep.32285 (2021).
33. Zhang, M., Wang, G. & Peng, T. Calpain-mediated mitochondrial damage: An emerging mechanism contributing to cardiac disease. *Cells* https://doi.org/10.3390/cells10082024 (2021).
34. Miyazaki, T. & Miyazaki, A. Dysregulation of calpain proteolytic systems underlies degenerative vascular disorders. *J. Atheroscler. Thromb.* **25**, 1–15. https://doi.org/10.5551/jat.RV17008 (2018).
35. Ge, W. *et al.* Mep1a contributes to Ang II-induced cardiac remodeling by promoting cardiac hypertrophy, fibrosis and inflammation. *J. Mol. Cell Cardiol.* **152**, 52–68. https://doi.org/10.1016/j.yjmcc.2020.11.015 (2021).
36. Letavernier, E. *et al.* The role of calpains in myocardial remodelling and heart failure. *Cardiovasc. Res.* **96**, 38–45. https://doi.org/10.1093/cvr/cvs099 (2012).
37. Feng, R., Du, W., Lui, P., Zhang, J. & Liu, Y. CAPN2 acts as an indicator of hepatitis B virus to induce hepatic fibrosis. *J. Cell Biochem.* **121**, 2428–2436. https://doi.org/10.1002/jcb.29465 (2020).
38. Sato, T. *et al.* Fibrosis resolution in the mouse liver: Role of Mmp12 and potential role of calpain 1/2. *Matrix Biol. Plus* **17**, 100127. https://doi.org/10.1016/j.mbplus.2022.100127 (2023).
39. Fengler, V. H. *et al.* Susceptibility of different mouse wild type strains to develop diet-induced NAFLD/AFLD-associated liver disease. *PLoS ONE* **11**, e0155163. https://doi.org/10.1371/journal.pone.0155163 (2016).
40. Gallou-Kabani, C. *et al.* C57BL/6J and A/J mice fed a high-fat diet delineate components of metabolic syndrome. *Obesity* **15**, 1996–2005. https://doi.org/10.1038/oby.2007.238 (2007).
41. Poussin, C. *et al.* Oxidative phosphorylation flexibility in the liver of mice resistant to high-fat diet-induced hepatic steatosis. *Diabetes* **60**, 2216–2224. https://doi.org/10.2337/db11-0338 (2011).
42. Tan, M. *et al.* Chronic subhepatotoxic exposure to arsenic enhances hepatic injury caused by high fat diet in mice. *Toxicol. Appl. Pharmacol.* **257**, 356–364. https://doi.org/10.1016/j.taap.2011.09.019 (2011).
43. Isaacson, R. H. *et al.* Olanzapine-induced liver injury in mice: Aggravation by high-fat diet and protection with sulforaphane. *J. Nutr. Biochem.* **81**, 108399. https://doi.org/10.1016/j.jnutbio.2020.108399 (2020).
44. Massey, V. L. *et al.* The hepatic "matrisome" responds dynamically to injury: Characterization of transitional changes to the extracellular matrix in mice. *Hepatology* **65**, 969–982. https://doi.org/10.1002/hep.28918 (2017).
45. Rittié, L. Method for picrosirius red-polarization detection of collagen fibers in tissue sections. *Methods Mol. Biol.* **1627**, 395–407. https://doi.org/10.1007/978-1-4939-7113-8_26 (2017).
46. Keshishian, H., Addona, T., Burgess, M., Kuhn, E. & Carr, S. A. Quantitative, multiplexed assays for low abundance proteins in plasma by targeted mass spectrometry and stable isotope dilution. *Mol. Cell. Proteomics* **6**, 2212–2229. https://doi.org/10.1074/mcp.M700354-MCP200 (2007).
47. Carr, S. A. *et al.* Targeted peptide measurements in biology and medicine: Best practices for mass spectrometry-based assay development using a fit-for-purpose approach. *Mol. Cell. Proteomics* **13**, 907–917. https://doi.org/10.1074/mcp.M113.036095 (2014).
48. Merchant, M. L. *et al.* Proteomic analysis identifies distinct glomerular extracellular matrix in collapsing focal segmental glomerulosclerosis. *J. Am. Soc. Nephrol.* **31**, 1883–1904. https://doi.org/10.1681/asn.2019070696 (2020).
49. Liu, H., Lafferty, J. & Wasserman, L. The nonparanormal: Semiparametric estimation of high dimensional undirected graphs. *J. Mach. Learn. Res.* https://doi.org/10.1145/1577069.1755863 (2009).
50. Sedgewick, A. J. *et al.* Mixed graphical models for integrative causal analysis with application to chronic lung disease diagnosis and prognosis. *Bioinformatics* **35**, 1204–1212. https://doi.org/10.1093/bioinformatics/bty769 (2019).

Acknowledgements

Supported, in part, by grants from NIH (R01 DK130294, R01 AA021978, P20 GM113226, P30 DK120531).

Author contributions

J.L.: visualization, investigation, validation, formal analysis, writing-original draft. T.S., J.I.B.: investigation, validation, formal analysis. M.H.-T.: writing-original draft. K.S.: visualization, formal analysis, writing-original draft. P.V.B., M.L.M., A.D.-R.: visualization, conceptualization, supervision, writing-original draft, funding acquisition, resources. D.W.: investigation, validation. A.H.: formal analysis, resources. A.W.: formal analysis. G.E.A.: project administration, visualization, conceptualization, investigation, supervision, writing-review and editing, funding acquisition, resources.

Competing interests

The authors declare no competing interests.

Additional information

Supplementary Information The online version contains supplementary material available at https://doi.org/10.1038/s41598-023-36867-x.

Correspondence and requests for materials should be addressed to G.E.A.

Reprints and permissions information is available at www.nature.com/reprints.

Publisher's note Springer Nature remains neutral with regard to jurisdictional claims in published maps and institutional affiliations.